FUZZY MRF MODELS WITH MULTIFRACTAL ANALYSIS FOR MRI BRAIN TISSUE CLASSIFICATION

Liang Geng and Weibei Dou
Department of Electronic Engineering, Tsinghua University, Beijing, P. R. China

Keywords: Brain tissue classification, Fuzzy MRF Model, multifractal analysis.

Abstract: This paper introduces multifractal analysis to the Fuzzy Markov Random Field (MRF) Model, used for brain tissue classification of Magnetic Resonance Images (MRI). The traditional classifying method using Fuzzy MRF Model is already able to calculate out the memberships of each voxel, to solve the Partial Volume Effect (PVE). But its accuracy is relatively low, for its spatial resolution is not high enough. Therefore the multifractal analysis is brought in to raise the accuracy by providing local information. The improved method is tests on both simulated data and real images, where results on membership average errors and position errors are calculated. These results show that the improved method can provide much higher accuracy.

1 INTRODUCTION

Magnetic Resonance Images (MRI) have been widely used for brain diagnosis and disorder detections. Accordingly, segmenting brain images into different tissues, such as cerebrospinal fluid (CSF), grey matter (GM) and white matter (WM), for clinical uses, has become a classical problem.

Many different tissue segmenting methods and algorithms are proposed these years. Some methods are using T1 weighted images (Rajapakse *et al*, 1996), while others use multispectral MR data (Taxt and Lundervold, 1994). Algorithms can be based on histogram determination Suzuki and Toriwaki, 1991), or on a priori information on anatomy (Joliot and Mazoyer, 1993). Mathematical models are used, from cluster analysis (Simmons *et al*, 1994) to Bayesian estimation (Chang *et al*, 1996). All these methods assume that each voxel in the images to be segmented belongs to only one specific tissue. However, due to the partial volume effect (PVE), one voxel may contain information from several different tissues, flawing the segmenting results of the methods proposed.

To solve the effect of PVE, Markov Random Field (MRF) Model is applied to tissue classification (Ruan and Cyril *et al*, 2000). The a priori information from an image and the classifying criteria are combined into energy functions of MRF's distribution, and then the voxels with mixed tissues can be classified by the iterated conditional mode (ICM). This method achieves a so-called 'Hard Classifying', classifying each voxel into one tissue who contributes the most, and contributions from other tissues are neglected. Considering that the neglected information is usually useful, a further model, the Fuzzy MRF Model, is brought in (Ruan and Moretti *et al*, 2001). The Fuzzy MRF Model takes into account the contextual information, the statistical information and the anatomical information of the brain. And 'Hard Classifying' is replaced by 'Fuzzy Classifying', providing 'memberships' for each voxel, indicating each voxel's partial volume degree, in other words, representing how much these tissues occupy one voxel respectively.

The fuzzy MRF Model is proved effective on PVE, but still limitations it has. Experiments show that this method performs poorly at brinks of brain images, where grey-level of voxels changes suddenly, which implies its spatial resolution is not high enough. Also, this method being noise sensitive, when it encounters images with high noise, its accuracy becomes even worse. These limitations can be attributed to the lack of local properties extracted from images, so what we need to do is to provide the Fuzzy MRF abundant local information.

As a new signal processing method, multifractal analysis is competent for this object. Multifractal is

Geng L. and Dou W. (2008).
FUZZY MRF MODELS WITH MULTIFRACTAL ANALYSIS FOR MRI BRAIN TISSUE CLASSIFICATION.
In *Proceedings of the First International Conference on Bio-inspired Systems and Signal Processing*, pages 33-39
DOI: 10.5220/0001064400330039

first studied mathematically (Halsey *et al*, 1986), and introduced to image processing by Sarkar and Katsuragawa (1995). It has derived various methods for image analysis, and has shown its advantages in local feature extraction (Liu and Li, 1997). It is also adapted to MRI brain tissue classifying, to remove ambiguities in the 'Hard Classifying' caused by intensity overlap, and performed well (Ruan *et al*, 2000)

Our research aims to raise the spatial resolution by local information while using fuzzy MRF model. We propose a combining both fuzzy MRF model and multifractal analysis together, to achieve a more accurate 'Fuzzy Classifying'. In this paper, we firstly show an overall of the proposed scheme and two kenel algorithms, fuzzy MRF and multifractal analysis, then explain how to combine these two parts in section 2. The validation of this improved scheme is done both by some experiments and in comparison with traditional fuzzy MRF method. The results and discussion are shown in section 3. This improved algorithm takes the same frame as the original method, while changes are done mathematically. Experiments and tests are done on various images, including real and virtual data with different amount of added noise.

2 ALGORITHMS

In this section we will introduce the algorithms for Fuzzy MRF Model along with multifractal analysis. We will show how the Fuzzy MRF Model works and how the multifractal information improves its classifying results.

2.1 A Whole Algorithm for Fuzzy MRF Model with Multifractal Analysis

Here we give out the flowchart of the whole algorithm using Fuzzy MRF Model with multifractal analysis, as Figure 1.

A parallel treatment, such as a preteatment for the parameter estimation of Fuzzy MRF Model and a multifractal analysis for producing a novel parameter U_3 to adjust a traditional Fuzzy MRF Model, is the contribution of this scheme.

The region framed by dashed line rectangle is the multifractal part added to the original frame. The other modules form the ICM iteration of Fuzzy MRF (Ruan and Moretti *et al*, 2001), and the multifractal part provides a 'tendence' to instruct the iterating course. We will discuss them in detail in following subsections.

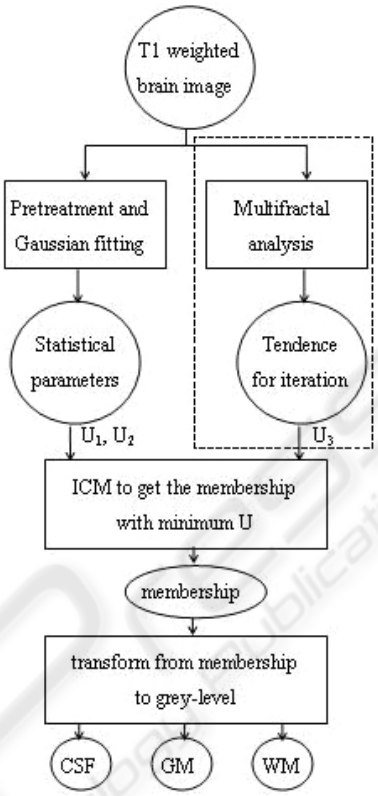

Figure 1: Flowchart of the whole algorithm.

2.2 Fuzzy MRF Model

The MRF Model is an a priori model, it represents the spatial correlation of image data. Considering a random field A with its realization a, in practice we usually use the joint probability density function of A on the whole image. Particularly when the probability density is distributed Gibbsian, the density function takes form as (1):

$$P(X=x)=\frac{1}{Z}\exp(-U(x)),\qquad Z=\sum_{x}\exp(-U(x)) \tag{1}$$

where $U(a)$ stands for the energy function, and Z the normalizing constant.

Fuzzy MRF Model applied to image segmentation, there are two random fields. One is the membership field A, whose realization is a, the other is the grey-level field Y, whose realization is y, which is known a priori. The goal of tissue classifying is to achieve the maximum joint probability density distribution of these two random field:

$$a_{result} = a \mid \{P_{A|Y}(a,y) \geq P_{A|Y}(x,y),\ \forall x\} \qquad (2)$$

The joint probability can be represented by conditional probability as:

$$P_{A,Y}(a,y) = P_A(a)P_{Y|A}(y \mid a) \qquad (3)$$

Comparing (1) and (3), we can get the probability distribution of Fuzzy MRF of image:

$$P_{A,Y}(a,y) = \frac{1}{Z}\exp(-U_1(a,y) - U_2(a)) \qquad (4)$$

Here U_1 represents the incompatibility between the grey-levels and the memberships, and U_2 represents the inhomogeneity of memberships themselves. They can be calculated using statistical parameters, which are acquired by fitting the grey-level histogram with several Gaussian functions (Ruan and Jaggi *et al*, 2000).

Once the two parts of energy function are calculated out, we can use the deterministic relaxation iterated conditional modes (ICM) to find the optimum realization of membership a, to ensure the energy function U being minimum, which means the joint probability in (1) being maximum.

The original algorithm concerns only these two parts of energy function, and information about the partial details are not taken into account. So we can see the shortcome of the original algorithms clearly by calculating the set-difference between classifying resluts and standard modules. Here we use a noise-free virtual image of normal brain with no RF. The original image is shown in Figure 2. Classifying results are shown in Figure 3 and differences in Figure 4, as we can see, the spatial differences mainly locate on the brinks, stings and nicks of the image, where grey level changes suddenly. If we could provide the algorithm enough local information to raise its spatial resolution, the result should be more accurate.

2.3 Multifractal Analysis

The multifractal analysis is first adopted into 'Hard Classification' by Ruan (Ruan and Bloyet, 2000), to remove the ambiguity caused by intensity overlap. The intensity overlap has nothing to do with the fuzzy model, since in fuzzy circumstances, we need not to reclassify a mixed voxel into one particular pure tissue. But the local information provided by multifractal still helps in raising the spatial resolution, thus we introduce the multifractal method to the Fuzzy MRF Model.

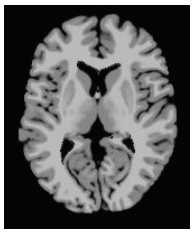

Figure 2: The original image named Vn00.

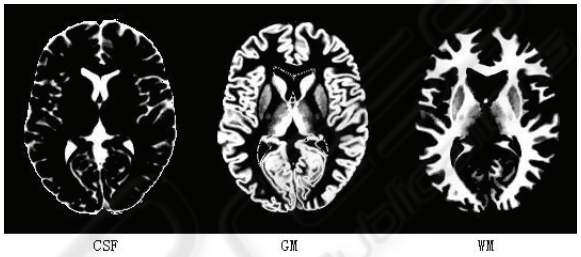

Figure 3: The classifying results of a virtual image.

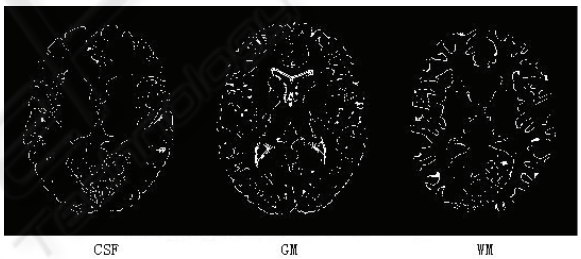

Figure 4: The spatial difference between classifying results and standard modules of a virtual image.

2.3.1 Multifractal in Signals

It is well known that fractal is widely used to process self-similar signals, by providing its global information of similarity to the 'fractal dimension'. But to provide local information, we need the 'fractal dimension' to vary from part to part of the signal. This is multifractal.

Therefore Multifractal dimension is defined locally by the measurement and length of a shrinking small region, as (5):

$$\alpha = \lim_{a \to 0} \frac{\log b}{\log a} \qquad (5)$$

where α denotes the multifractal dimension, also called Hölder exponent, b denotes the measurement, and a the length of the region.

Each small region has its own Hölder exponent, and then the whole signal can be considered as the union of many subsets that combining with each other. To characterize the local characteristics, we need another parameter to decompose these small regions, and group all voxels being in the same kind of detail into a set. The parameter brought in is called 'multifractal spectrum', defined as $f(\alpha)$. $f(\alpha)$'s definition can be Hausdorff, Legendrea, or others. We can also define it particularly.

2.3.2 Multifractal in Brain Images

To describe the local details of brain images, first we need to abstract these details into several simple models. Observe the images, we can find out three kinds of details shown in Figure 5.

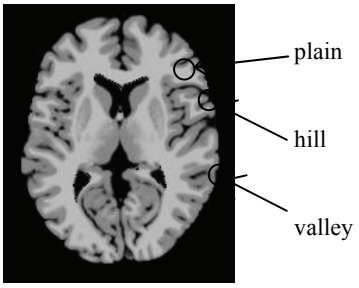

Figure 5: The details of brain image.

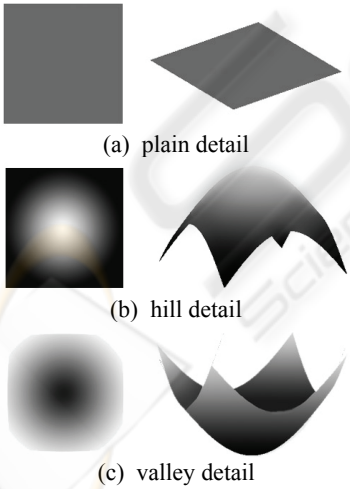

Figure 6: The models of details. The intensity model is on the left, while grey-level model is on the right.

Grey levels of voxels in plain region has little difference from the central voxel, most of the small regions are proved to be plain. Hill region has several voxels much lighter in the centre, and valley region has a much darker centre. The models can be illustrated as Figure 6.

After defined the three detail models, the Hölder exponent α is ready to be calculated out for each model. From the equation (5) we could know that α is defined to be a limit process. Because the image is composed by discrete voxels, the values of length *a* must also be discrete, thus the limit process is discrete: first *a* takes the radius of the small region *R* as its value, then each time *a* minus 1 until *a* becomes 0. The corresponding value of *b* is the sum of grey level of voxels in a diminishing spherical small region whose radius is *a*. Both *a* and *b* gotten, the Hölder exponent α can be gotten in succession. Since we only care about the relative size of the Hölder exponent α, the values themselves make no sense to us; we can also use some approximate method, such as linear fitting, instead of the complicate limit process.

At last, we can get the relative size of the Hölder exponent α in different details: for hill, α is relatively smaller, and for valley, α is relatively bigger, while for plain, it's in the middle.

To decompose image details and group the voxels into three sets, $f(\alpha)$ needs to be generated from α. And for concision, we define $f(\alpha)$ as α's histogram, that means:

$$f(\alpha_i) = \sum_{k \in I} \delta(\alpha(k), \alpha_i) \qquad (6)$$

where I represents the whole image, $\alpha(k)$ is the Hölder exponent at voxel k, $\delta(\alpha(k), \alpha_i)$ is Kronecker Function, which takes the value 1 while $\alpha(k) = \alpha_i$, and 0 while $\alpha(k) \neq \alpha_i$.

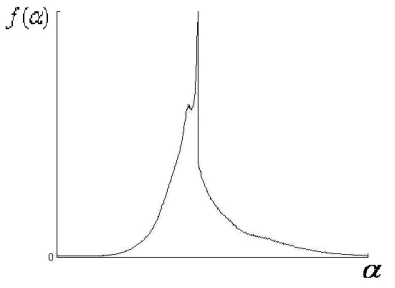

Figure 7: Multifractal spectrum of MR brain image.

Then we get the histogram as spectrum, shown in Figure 7. A correctly collected MR Brain image must has a multiractal spectrum in this shape, because most voxels are in plain regions, which makes the high peak in the middle. Therefore we need only to find the position of the peak, denoted as

α_0, representing the corresponding voxels being in plain detail, and voxels with an α smaller than α_0 are in hill regions, others are in valley regions.

2.4 Multifractal Applied to Fuzzy MRF

Using multifractal, we can label every voxel the detail type it belongs to, and the rest to be done is to combine the multifractal and Fuzzy MRF together, by influencing the ICM iterating process with these detail labels.

We consider translating the labels into some sort of 'tendence'. If a voxel is labelled 'hill', that means it's brighter than its neighbours, then it should have a tendence to be classified into a brighter tissue. If the voxel is labelled 'valley', on contrary, it should have a tendence to be classified into a darker tissue. If the voxel is labelled 'plain', its brightness is almost the same as its neighbours', so it should have no tendence.

Then the main problem is how to translate the detail labels into 'tendences'. Here we propose the 3rd energy function U_3, to change the value of U, therefore to impose the 'tendence' to the iterating process. From to gradient label (denoted by D), then to U_3, can be defined as equation (7):

$$D=\begin{cases}1 & \alpha<\alpha_{hill} \quad (hill)\\ 0 & \alpha_{hill}\le\alpha\le\alpha_{valley}\ (plain)\\ -1 & \alpha>\alpha_{valley} \quad (valley)\end{cases},$$
$$U_3 = D\cdot\beta_{fractal}\cdot\begin{cases}-1 & a>a_{current}\\ 0 & a=a_{current}\\ 1 & a<a_{current}\end{cases},\ \beta_{fractal}>0, \qquad (7)$$

For equation (7), α_{hill} and α_{valley} are thresholds generated from the spectrum $f(\alpha)$ shown in Figure 7, e.g, $\alpha_{hill}=\max(\alpha\mid f(\alpha)<f(\alpha_0)/2\ \&\ \alpha<\alpha_0)$ and $\alpha_{valley}=\min(\alpha\mid f(\alpha)<f(\alpha_0)/2\ \&\ \alpha>\alpha_0)$. And $\beta_{fractal}$ is a positive weight coefficient for U_3, whose value depends on how much you want the multifractal part to affect the whole system.

Using (7), the detail 'hill' can make U with brighter membership a smaller, and U with darker membership a bigger. For the detail 'valley', the performance is on the contrary. Thus multifractal can be applied to the algorithm frame shown in Figure 1.

3 EXPERIMENTS AND RESULTS

3.1 Experiment Materials

Experiments are done on 9 data sets to test the improved algorithm. These 9 sets of data includes various conditions, such as virtual data and real images, data with different noise levels and RF levels, data of normal brains and brains with defect. We name each image the way as following. The 1st letter indicates its source in V (virtual) and R (real). The 2nd letter indicates the defect of the brain, in n (normal), s (multiple sclerosis) and t (tumour). The 1st number indicates its noise level in percent. And the 2nd number indicates whether RF is added, in 1 if added or 0 if not.

The information of the 9 sets of data is listed in Table 1.

Table 1: Information of data sets used for tests.

Name	Source	Defect	Noise	RF
Vn00	virtual	normal	0%	0%
Vn30	virtual	normal	3%	0%
Vn50	virtual	normal	5%	0%
Vn70	virtual	normal	7%	0%
Vn01	virtual	normal	0%	20%
Vn71	virtual	normal	7%	20%
Vs00	virtual	multiple sclerosis	0%	0%
Rn	real	normal		
Rt	real	tumour		

To quantify the tests of accuracy, we mainly use the virtual data and their standard modules. The virtual data is from Montréal Neurological Institute, McGill University, McConnell Brain Imaging Centre (Website: http://www.bic.mni.mcgill.ca/brainweb/).

3.2 Evaluating Method

The classifying results of virtual images are evaluated in two ways. The 1st way is the position error e_p, which is the number of voxels classified differently from the standard module. The position error is defined as equation (8).

$$e_p = \sum_{(i,j,k)\in I} \delta(a_{result(i,j,k)}, a_{std(i,j,k)})$$

$$\delta(a_{result(i,j,k)}, a_{std(i,j,k)}) = \begin{cases} 1 & a_{result(i,j,k)} = a_{std(i,j,k)} \\ 0 & a_{result(i,j,k)} \neq a_{std(i,j,k)} \end{cases} \quad (8)$$

And the 2nd way is the membership average error e_m, which indicates the average error of memberships from the whole images. The membership average error is defined as equation (9), where N(I) represents the number of voxels.

$$e_m = \frac{\sum_{(i,j,k)\in I} \left| a_{result(i,j,k)} - a_{std(i,j,k)} \right|}{N(I)} \quad (9)$$

3.3 Result and Discussion

The position error of each image data using each algorithm is listed in Table 2, the membership average errors are listed in Table 3.

Both Table 2 and Table 3 show that the algorithm with multifractal has lower errors, in other words, higher accuracy than the original one. (In spite of some exceptions caused by noise and RF, such as GMs of Vn50 and Vn01 in Table 2, the flaws can be compensated by better results on the other tissues.)

Table 2: Position errors of two algorithms.

Data	Multi-fractal	e_p (number of voxels)		
		CSF	GM	WM
Vn00	without	68232	105738	55071
	with	66398	98904	54122
Vn30	without	114829	140443	139721
	with	115507	134358	139774
Vn50	without	188361	193855	223821
	with	183362	194035	222067
Vn70	without	228503	238072	281032
	with	228273	230507	278875
Vn01	without	165458	255996	195482
	with	166628	256531	190323
Vn71	without	232630	256904	306778
	with	232336	250765	302827
Vs00	without	72145	124560	72968
	with	72170	119322	69315

Table 3: Membership average errors of two algorithms.

Data	Multi-fractal	e_m		
		CSF	GM	WM
Vn00	without	1.6322	3.3685	1.3824
	with	1.5104	3.1752	1.3422
Vn30	without	2.1395	4.9949	2.7958
	with	2.0264	4.8018	2.7688
Vn50	without	2.9763	7.4779	4.6330
	with	2.8443	7.2597	4.5960
Vn70	without	4.3948	9.4826	5.9437
	with	3.5422	9.1410	5.9312
Vn01	without	2.3392	6.2700	3.9262
	with	2.2365	6.1273	3.8102
Vn71	without	3.8495	10.526	7.0626
	with	3.6663	10.136	7.0032
Vs00	without	1.6992	3.4159	1.4649
	with	1.6233	3.2771	1.4197

Because of the effect of other tissues such as muscles and bones, the errors are still not very low, but we could observe just the voxels at brinks, which we care about. Comparing the result images, we find that the voxels improved are mainly what we wanted to improve. Compare to the results from original method, the results of multifractal method have much less error voxels at the brinks of images. One comparison of position error using Vn00, the same data as Figure 2, is shown in Figure 8.

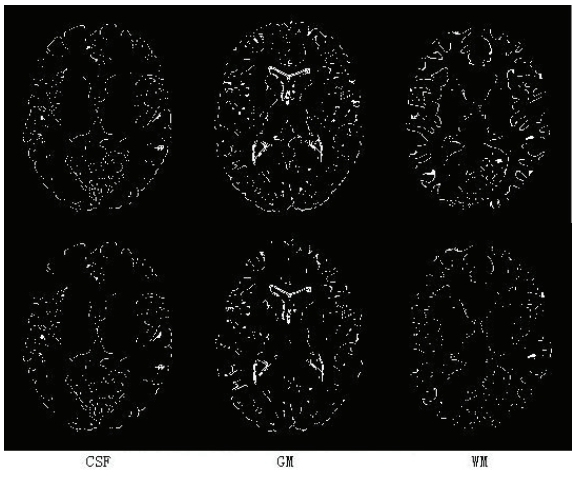

Figure 8: Position error of original algorithm (above) and improved algorithm with multifractal (below).

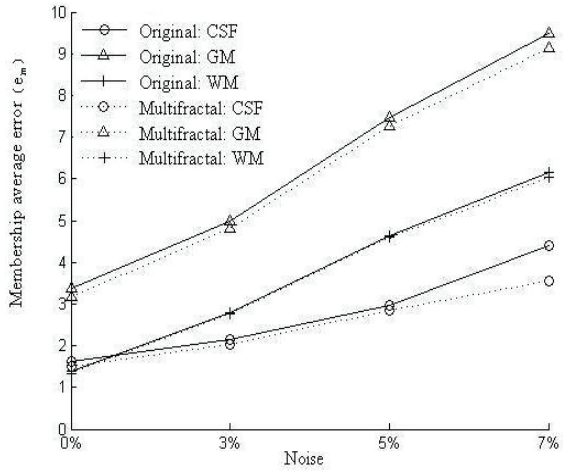

Figure 9: Membership average error of original algorithm (real line) and improved algorithm with multifractal (dotted line).

Another improvement is the better robustness on noise. We chart the average errors of Vn00 to Vn07 in Table 2, the curves are shown in Figure 9.

The higher the noise level becomes, the greater the accuracy improves. The improved method with multifractal is improved less sensitive to noise, and can be used to contain the deterioration caused by high noise.

Results of real image Rn and Rt have been compared to some manual segmenting results, and they match each other. The improved method can be well used for real applications.

4 CONCLUSIONS

An improvement from multifractal analysis has been done to the traditional tissue classifying algorithm using Fuzzy MRF Model. The original mathematical models and fuzzy features are reserved, when spatial resolution is increased, thus accuracy is improved. In numbers of tests on various sorts of data, the improved method shows its advantage on accuracy to the original method. Also an entire algorithm using the improved method is proposed and tested, doing well in real applications.

ACKNOWLEDGEMENTS

This work is supported by Project NSFC-60372023, the National Natural Science Foundation of China. We would like to give special thanks to Su Ruan, Jean-Marc Constans and Lab of GREYC-ENSICAEN CNRS UMR 6072 of France for providing us their research experience and experimental code.

REFERENCES

Rajapakse, J.C., Giedd, J.N., DeCarli, C., Snell, J.W., McLaughlin, A., Vauss, Y.C., Krain, A.L., Hamburger, S., Rapoport, J.L., 1996. A technique for single channel MR brain tissue segmentation: application to a pediatric sample. *Magn Res Imag*, 14, 1053~1065.

Taxt, T., Lundervold, A., 1994. Multispectral analysis of the brain using magnetic resonance imaging. *IEEE Trans Med Imag*, 13, 470~481.

Suzuki, H., Toriwaki, J., 1991. Automatic segmentation of head MRI images by knowledge guided thresholding. *Comput Med Imag Graph*, 15, 233~240.

Joliot, M., Mazoyer, B., 1993. Three-dimensional segmentation and interpolation of magnetic resonance brain images. *IEEE Trans Med Imag*, 12, 269~277.

Simmons, A., Arridge, S.R., Barker, G.J., Cluckie, A.J., Tofts, P.S., 1994. Improvement to the quality of MRI cluster analysis. *Magn Res Imag*, 12, 1191~1204.

Chang, M.M., Sezan, M.I., Tekalp, A.M., Berg, M.J., 1996. Bayesian segmentation of multislice brain magnetic resonance imaging using threedimensional Gibbsian Priors. *Optical Engineering*, 35, 3206~3221.

Ruan, S., Jaggi, C., Xue, J., Fadili, J., Bloyet, D., 2000. Brain Tissue Classification of Magnetic Resonance Images Using Partial Volume Modeling. *IEEE Trans Med Imag*, 19, 1179~1187.

Ruan, S., Moretti, B., Fadili,J., and Bloyet, D., 2001. Segmentation of Magnetic Resonance Images using Fuzzy Markov Random Fields. *IEEE*, 3, 1051~1054.

Halsey, T.C., Jensen, M.H., Kadanoff, L.P., Procaccia, I., Shraiman, B.I., 1986. Fractal measures and their singularities, the characterization of strange sets. *Phys. Rev.*, 33, 1141–1151.

Sarkar, N., Katsuragawa, S., 1995. Multifractal and generalized dimension of gray-tone digital images. *Signal Processing*, 42, 181~190.

Liu, Y., Li, Y., 1997. New approaches of multifractal image analysis. *IEEE-ICICS' 1997*, 2, 970~974.

Ruan, S., Bloyet, D., 2000. MRF Models and Multifractal Analysis for MRI Segmentation. *IEEE-ICSP'2000*, 2, 1259~1262.